ACS Photonics

Article

Cite This: ACS Photonics XXXX, XXX, XXX−XXX

pubs.acs.org/journal/apchd5

Nonlinear Spectroscopy on the Plasmonic Analog of Electromagnetically Induced Absorption: Revealing Minute Structural Asymmetries

Joachim Krauth,*[,†] Thorsten Schumacher,[‡] Josselin Defrance,[†] Bernd Metzger,[†] Markus Lippitz,[‡] Thomas Weiss,[†] Harald Giessen,[†] and Mario Hentschel[†]

[†]4th Physics Institute and Research Center SCoPE, University of Stuttgart, Pfaffenwaldring 57, 70569 Stuttgart, Germany

[‡]Experimental Physics III, University of Bayreuth, 95447 Bayreuth, Germany

Supporting Information

ABSTRACT: Tailoring not only the linear but also the nonlinear properties of plasmonic structures has been a longstanding idea. The plasmonic dolmen structure with its many degrees of freedom in design has been of particular interest. We are investigating this system in detail in the retarded weak-coupling regime, the so-called plasmonic analog of electromagnetically induced absorption. While it is generally expected that the enhanced absorbance leads to an increased nonlinear generation, we find that the details are more complex. A thorough wavelength and polarization resolved study reveals two distinct nonlinear contributions. Our nonlinear spectroscopy method exhibits a surprisingly high sensitivity to minute structural asymmetries. Our experimental results are corroborated by finite-element simulation. We envision that our findings will stimulate further research into phase tuning, structural symmetries, and manipulation in nonlinear plasmonic systems in order to fully exploit the ability to tailor the linear and specifically the nonlinear optical properties of the nanostructured matter.

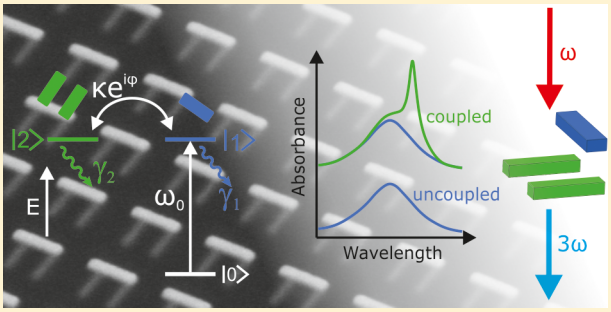

KEYWORDS: *nonlinear plasmonics, spectroscopy, nonlinear spectroscopy, structural asymmetry, 3D nanostructure, electromagnetically induced absorption*

In recent years, advances in the nanofabrication processes enabled the investigation of a vast variety of different nanostructures designed in order to tailor or attempt to tailor the linear and nonlinear properties of plasmonic systems,[1−4] ranging from rod antennas,[5] split-ring resonators,[6,7] bowtie antennas[8−10] to more complex structures such as oligomers,[11,12] twisted-crosses,[13] metamaterials,[14,15] and metasurfaces.[16,17] In the course of these investigations, second harmonic generation (SHG),[7,18−20] third harmonic generation (THG),[5,21,22] and four-wave mixing (FWM)[23−26] have been performed on single nanostructures[27−31] as well as on arrays.[32−35] The materials of choice varied from noble metals such as gold or silver[36] to the implementation of semiconductors to plasmonic systems[37,38] as the appropriate choice of the material offers an additional tuning parameter of the optical response. Of particular interest has been the hybridization of two or more modes in such structures.[39−44]

The nonlinear conversion efficiencies are linked to the quality factor of the utilized modes and therefore to their intrinsic line width and local near-field strength.[10] So-called plasmonic dark modes are thus of particular interest as they exhibit the largest field enhancements. However, these modes cannot be excited by incident plane waves due to a zero net dipole moment. Importantly, due to reciprocity, they also cannot radiate to the far-field. Consequently, in order to benefit from the favorable properties of these dark modes, in- and out-coupling of far-field energy is required. The general idea to achieve this relies on plasmon hybridization, that is, the near-field mediated coupling between a bright and a dark plasmonic mode. One archetype system is the so-called plasmonic dolmen structure depicted in Figure 1. The structure consists of a single rod antenna stacked on top of a pair of rod antennas that are rotated by 90° with respect to the single rod. If designed correctly, the bright dipolar resonance of the rod energetically coincides with the dark out-of-phase oscillation of the dipolar modes (the quadrupolar mode) of the nanorod pair. The hybridization of these modes leads to the emergence of two resonances in the far-field spectrum for light polarized along the dipolar antenna. These modes split around the common resonance wavelength of the original modes, opening a transmittance window at the position of the former transmittance minimum of the bare dipolar rod antenna. This phenomenon has therefore been compared with the atomic physics concept of electromagnetically induced transparency (EIT) and has been coined its plasmonic analog.[45] The main

Received: July 1, 2019
Published: October 9, 2019

DOI: 10.1021/acsphotonics.9b00938
ACS Photonics XXXX, XXX, XXX−XXX

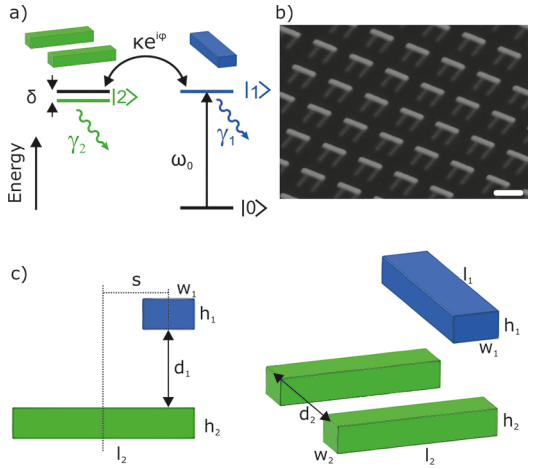

Figure 1. (a) Mode coupling scheme of the EIA structure. A direct excitation is solely possible for the dipolar mode $|1\rangle$. The quadrupolar ($|2\rangle$) and dipolar mode are coupled via the complex coupling constant κ. (b) Tilted scanning electron microscope overview image of the nanoantenna array. The scale bar is 400 nm. (c) Geometry of the 3D plasmonic structure. The dimensions of the dipole rod are l_1 = 450 nm, w_1 = 120 nm, h_1 = 60 nm, and the dimensions of the quadrupole rods are l_2 = 400 nm, w_2 = 80 nm, h_2 = 40 nm. The vertical distance d_1 = 120 nm and the center-to-center distance d_2 = 270 nm. The displacements of the dipole ranges from 0 to 140 nm.

benefit afforded lies with the optical access to the dark mode. The new hybridized modes "inherit" the properties of the original modes, and consequently, the quality factor of these new modes is higher compared to the dipolar resonance. The new modes can therefore be considered "partially dark," since energy that is stored in the originally dark quadrupole mode can thus be exchanged between the mode and the far-field.

The coupling of the plasmonic modes and the resulting spectral features can also be understood using the well-known energy level diagram in direct analogy to atomic physics, as depicted in Figure 1a. The dipolar mode of the single rod is a bright transition and is represented by the transition from state $|0\rangle$ to $|1\rangle$. The dark quadrupolar mode is represented by state $|2\rangle$ to which a dipolar transition is forbidden. A direct excitation from $|0\rangle$ by applying an external electromagnetic field at frequency ω_0 is only possible for the dipole mode $|1\rangle$ but not for state $|2\rangle$, which is associated with the two quadrupole rods. Both excited states offer a decay rate γ_1 and γ_2 for the dipole and quadrupole state, respectively, where γ_2 is much smaller due to the nonradiative nature of the mode. In general, state $|2\rangle$ of the quadrupole can be energetically detuned by the energy difference δ with respect to state $|1\rangle$. Coupling between the two excited states, in the most general case described by a complex coupling coefficient $\kappa e^{i\varphi}$, allows for the indirect excitation of the dark state $|2\rangle$. In atomic physics, the two distinct excitation paths of mode $|1\rangle$, namely, the direct excitation $|0\rangle \rightarrow |1\rangle$ and an indirect one $|0\rangle \rightarrow |1\rangle \rightarrow |2\rangle \rightarrow |1\rangle$, interfere. In the conventional EIT scheme, these two excitation paths interfere destructively, which leads to the opening of a transmission window, which also happens with its plasmonic analog.[45]

This concept has been used extensively over the last years and can also be transferred to other geometries, which might be structurally more complex, such as dense particle clusters or similar.[46,47] Other coupling mechanism of different modes reaching even into the strong coupling regime that have been investigated recently are, for example, the coupling of a nanoantenna resonance with a molecular vibration.[48] It is less well-known that the destructive interference in the case of plasmonic EIT can be turned into *constructive* interference by appropriate design of the coupling mechanism. In that case, one will in fact not observe an increased transmittance but an enhanced absorbance of the coupled system.[49] This phenomenon is termed the plasmonic analog of electromagnetically induced absorbance (EIA), as it is also known in atomic physics. In plasmonics, the phase tuning is achieved via retardation effects. If one increases the vertical distance between the dipole and the antenna pair, the so-called quasi-static approximation is no longer valid and a propagation induced phase shift φ can be accumulated. This behavior can in fact be captured by the complex coupling coefficient introduced earlier. Another example of such an anti-Hermitian coupling has been investigated on an array of densely positioned plasmonic nanoantennas, which allows for spatially manipulating light in the deep subwavelength scale.[50,51]

Recently, it has been suggested that such induced absorbance systems could be ideally suited for nonlinear optics. The reasoning is as follows: In bulk macroscopic nonlinear optics, large absorbance leads to high nonlinear signals as the absorbance is the key parameter characterizing conversion efficiencies. Microscopically speaking, the nonlinear susceptibility is determined by the linear absorbance of the systems being indicative of the optically excitable transition in the medium, which are capable of enhancing the conversion efficiency. In analogy, it has been suggested that the EIA structure should be an ideal plasmonic geometry for nonlinear experiments as it offers large absorbance and a simultaneously narrow line width due to the quadrupolar contributions to the observed resonances.[52]

We report third harmonic (TH) spectroscopy results on the EIA structure. As mentioned above, this structure should lead to large nonlinear signals as the absorbance is highly increased in such a plasmonic system. We analyze this model carefully in theory and experiment and extract a very detailed assessment of the nonlinear properties. In fact, the overall conversion efficiencies are similar to comparable plasmonic systems, such as planar dolmen structures. The nonlinear conversion efficiencies in plasmonic systems are governed by a number of different properties, which are the line width, the modulation depth, and the effective oscillator strength. Optimization of one quantity might be detrimental for another, and in our case, we deal most likely with a trade-off between line width and oscillator strength. In investigating the polarization state of the TH, we find that two distinct TH contributions of similar magnitude exist, one polarized along the dipole axis and one perpendicular to it. The latter is highly surprising as the coupled modes should not have any dipole moments perpendicular to the dipole antenna axis and should therefore not be able to radiate TH polarized along this direction.[53] We ascribe this observation to structural asymmetries, mainly a different length of the quadrupole antenna arms, which is barely detectable in the linear response. Interestingly, our nonlinear investigations of these complex plasmonic structures can help to detect very minute asymmetries in the system and reveal information more sensitively about the detailed structure than the linear optical response alone. Apart from the THG, we also observe weak SHG. In electric dipole approximation, SHG requires broken inversion symmetry of the system. The relative roles of broken

DOI: 10.1021/acsphotonics.9b00938
ACS Photonics XXXX, XXX, XXX−XXX

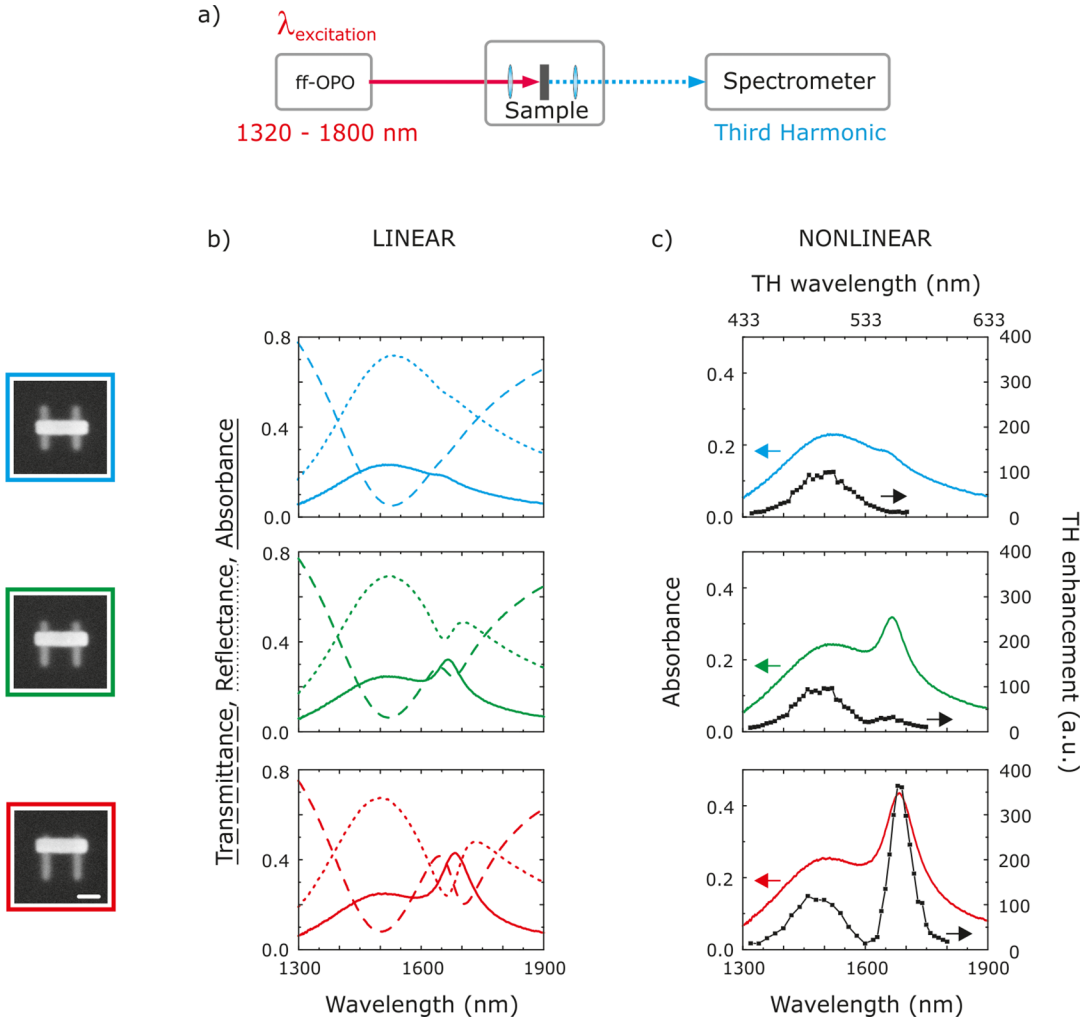

Figure 2. (a) Scheme of the experimental setup. (b) Linear spectra for the three different coupling strengths of the EIA structure. The dashed, dotted, and solid lines indicate transmittance, reflectance, and absorbance spectra, respectively. Blue SEM image, structure shows no coupling; green SEM image, coupling is introduced; red SEM image, coupling is maximized. With increased coupling, the second mode at 1700 nm due to the excitation of the quadrupole becomes more pronounced. This is most visible in the absorbance spectrum (solid lines). (c) Resulting nonlinear TH spectroscopy results. With emergence of the second mode in the absorbance spectrum, also the nonlinear response exhibits a second peak in the TH enhancement. This second TH peak at about 1700 nm is small for weak coupling (green) and is dominant when going to the largest coupling (red).

inversion symmetry in the design of the plasmonic structures and the influence of surface defects and imperfections are still under debate in the literature. Evidence for both phenomena has been reported.[1] These findings clearly merit further detailed investigations.

An exemplary tilted overview scanning electron microscope image of our nanostructure array is presented in Figure 1b. The nanoantenna arrays are fabricated using standard electron beam lithography on an ultraviolet transparent glass substrate. The different arrays have a size of 100 × 100 μm^2. The material of choice is gold as it offers high-quality resonances and chemical stability as well as ease of fabrication.[54,55] The dimensions of the plasmonic structures as shown in Figure 1c are as follows: the dipole antennas exhibit a nominal length of 450 nm, a width of 120 nm, and a height of 60 nm, while both lower rods forming the quadrupole are 400, 80, and 40 nm in length, width, and height, respectively. The vertical distance between both rod antennas is 120 nm and the center-to-center distance between the quadrupole rods is 270 nm. As spacer layer between the different layers, IC1-200 is used. In the *x*- and *y* directions, the periodicity of the single nanostructures is set to 700 nm to avoid coupling among the nanostructures and to shift Rayleigh anomalies out of the spectral region of interest. The coupling strength κ of the system is determined by the displacements of the dipole rod with respect to the center position of the quadrupole rods toward the end of the quadrupole arms and grows with increasing symmetry breaking by increasing the displacements.

Our experimental setup for the nonlinear spectroscopy is sketched in Figure 2a. A femtosecond Yb:KGW oscillator at a repetition rate of 44 MHz and 180 fs pulse duration[56] is used for pumping a fiber-feedback optical parametric oscillator (OPO).[57,58] The OPO signal output is used as exciting fundamental wave in our nonlinear spectroscopy measurement and offers a tuning range in the near-infrared from about 1320 to 1800 nm with pulse durations of around 200 fs. The resulting OPO signal pulses exhibit a Gaussian shape and are nearly Fourier-limited. More details can be found in Figure S1 of the Supporting Information. The output power is set to a constant level of 25 mW for all excitation wavelengths using a

DOI: 10.1021/acsphotonics.9b00938
ACS Photonics XXXX, XXX, XXX−XXX

neutral density filter disc wheel. In principle, more power could lead to an increased signal-to-noise ratio; however, it comes at the risk of sample degradation. Thus, the used value was found to be a good trade-off. The OPO beam is focused onto the sample with the polarization set along the dipole long axis (x direction) to ensure the most efficient excitation of the plasmonic system. In order to avoid parasitic TH signals that could be generated on optics used in the experimental setup and would influence the measurement results, a RG715/2 mm filter (Schott) is placed in front of the sample to eliminate this potential source of distortion. The generated TH signal in transmission is collected using a second lens and separated from the remaining OPO signal beam with a heat absorbing filter (Schott KG5/6 mm) and subsequently coupled into a spectrometer (Acton 2500). The spectrometer is equipped with a grating and a Peltier-cooled charge coupled device (CCD) camera (Pixis 256E) to detect the TH signal in the visible spectral range.

Figure 2b depicts the linear spectra (transmittance T, reflectance R, and absorbance A) of our investigated dolmen-type structure arrays. The three different panels represent the linear measurement results for three different coupling strengths, with increasing coupling from top to bottom. The transmittance and reflectance have been measured utilizing a Fourier-transform infrared (FTIR) spectrometer (Bruker Vertex 80), equipped with a microscope (Hyperion 3000). The resulting absorbance A can then be calculated using $A = 1 - T - R$.

In the uncoupled regime (blue bordered SEM image), we observe just a single plasmon resonance centered around 1500 nm, originating from the single dipole rod. When increasing the coupling strength by shifting the dipole rod out of the center position (green SEM image), a second mode is emerging. This mode is best visible when inspecting the absorbance spectrum. When further increasing the coupling strength (red bordered SEM image), this absorbance feature is further growing in amplitude. It is interesting to note that the transmittance, reflectance, and absorbance spectra have distinctly different shapes and relative amplitudes. By now, it is well established that the local field-enhancement and in particular the local linear dipole moments of the plasmonic resonances are the source of the nonlinear radiation. In most plasmonic systems, transmittance, reflectance, and absorbance follow very similar trends and therefore one can in fact not differentiate which describes the nonlinear response best. In the case of EIA, as clearly evidenced by the spectra, there are significant differences in between the spectra. The relative absorbance shows sizable changes around 1700 nm, whereas the relative changes in the transmittance are comparably small. The absorbance, or energy dissipation, is in fact most representative for the near-field enhancement in the plasmonic structure, and thus a correlation of the TH enhancement with the absorbance spectra that represent the linear optical susceptibility $\chi^{(1)}(\omega)$ of the sample is expected.

In order to further investigate these issues, we perform TH spectroscopy measurements on the three arrays with different coupling strengths. To obtain the full TH enhancement curve of our plasmonic structures, we sweep the OPO signal wavelength in steps of 10 nm from 1320 to 1800 nm over each linear spectrum, and the generated TH spectrum is recorded for each fundamental wavelength. We then spectrally integrate over each of the TH spectra to obtain a single scalar value describing the measured TH enhancement at each wavelength point. In order to account for slight variations of the pulse parameters (e.g., intensity or pulse duration) and any wavelength-dependent influence of the experimental setup (e.g., filters, detectors, or focusing optics), we additionally measure the generated TH intensity spectrum of a bare 5 mm thick glass substrate (avoiding the observed interference of the TH signal of the bare thin sample substrate) for each fundamental wavelength. These spectra are also spectrally integrated and then used as normalization for the previously measured TH spectra of our nanoarrays. In addition, the resulting TH intensities are multiplied by a wavelength-dependent factor accounting for the dispersion of the gold nonlinearity, which was obtained by measuring the TH response from a bare gold film and referencing it to the substrate.[59] We do not expect the substrate or the spacer layer of our sample to influence the TH measurement as their nonlinearity is comparably small.

The resulting TH enhancement curves as a function of the fundamental wavelength of our plasmonic sample with respect to the substrate are plotted in Figure 2c for the three different coupling strengths. Furthermore, each panel shows the respective absorbance spectrum. In the uncoupled case, we obtain a single peak in the nonlinear regime corresponding to the single dipole resonance with an enhancement factor of around 100 obtained at 1510 nm. With increasing coupling, we observe the emergence of a second peak with relatively small amplitude (around 30 at 1670 nm), which is associated with the second mode in the linear spectrum, while the first peak in the TH enhancement at around 1520 nm remains almost unchanged in spectral position and amplitude with an enhancement factor of around 100. For strongest coupling, we observe a sizable TH enhancement of about 365 at 1680 nm, corresponding to the second mode. This is a three times stronger signal than at the higher energy mode at around 1500 nm. In comparing the linear spectra, we find that the TH enhancement curve indeed follows the absorbance spectra. The mode at around 1680 nm exhibits the strongest TH enhancement, which matches with the significantly larger amplitude in the absorbance response of this mode compared to the higher energy mode. This behavior is not found in the transmittance nor reflectance spectra, which exhibit distinctive spectral features, as can be seen when closely inspecting the spectra in Figure 2b. Thus, our EIA scheme allows one to clearly corroborate the influence of the absorbance on the TH efficiency of the plasmonic structure. It should be noted that the linear absorbance spectra can also be fitted using a coupled harmonic oscillator model. This very simple model can quite easily estimate the TH response of the coupled system. For more information, please refer to the Supporting Information.

Next, we are inspecting the polarization state of the radiated TH response. We choose the array with the largest displacement and thus with the strongest coupling for this in-depth investigation. A polarizer is added between the sample and the spectrometer in order to resolve the polarization state at each wavelength point. We measure the TH signal of the EIA sample in dependence of the polarizer angle θ in steps of 10° from 0° to 360° and normalize each TH spectrum to the TH emitted from the bare substrate. For the reference measurement, the polarizer angle is set to 0°, corresponding to the x axis of our system and the polarization of the exciting fundamental electric field as the signal generated by the sample is known to be polarized along the fundamental light field. We would like to note that for the perfectly symmetric structure,

DOI: 10.1021/acsphotonics.9b00938
ACS Photonics XXXX, XXX, XXX−XXX

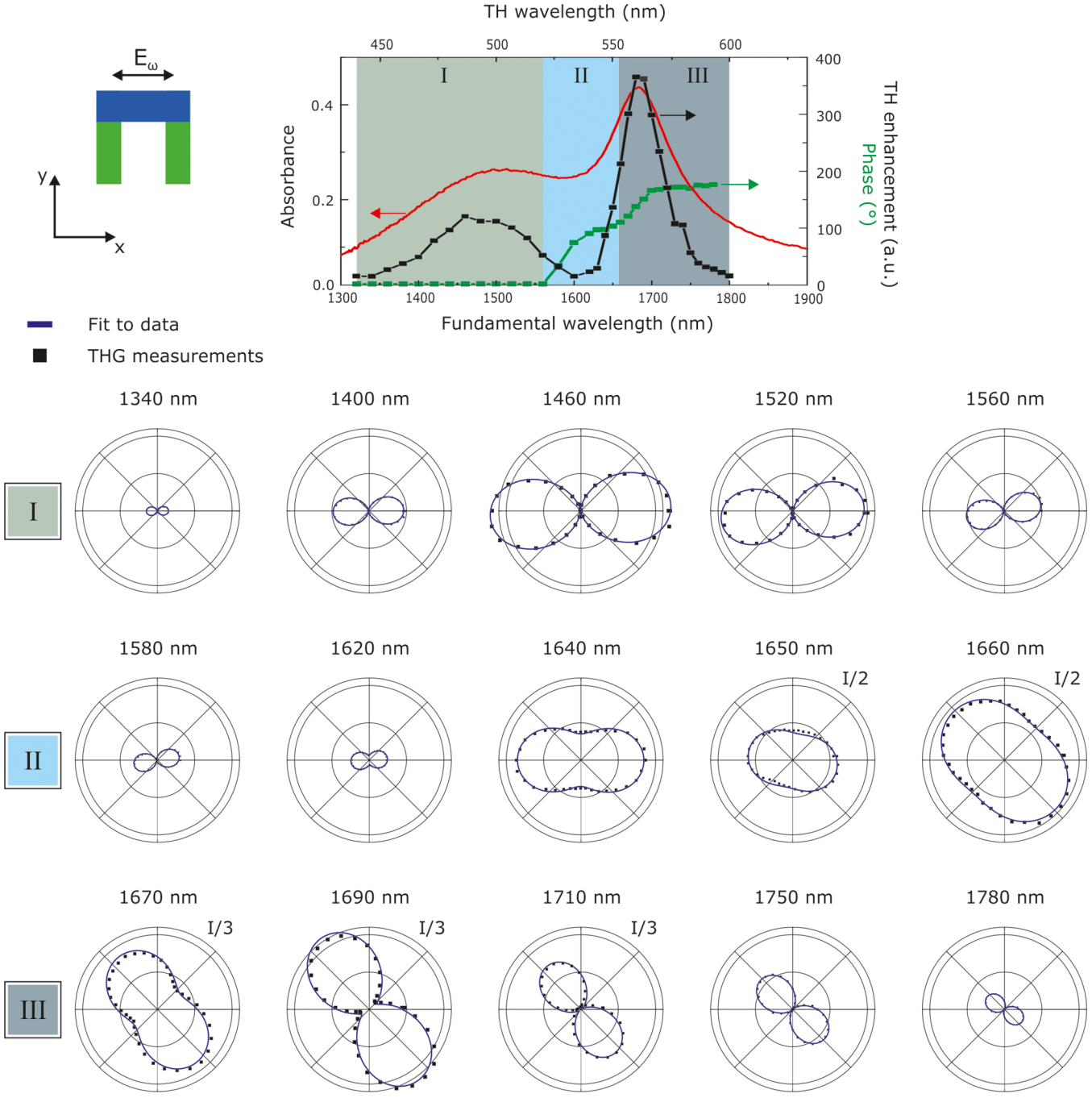

Figure 3. Top panel: TH spectroscopy results for the strongest coupling array. Lower panels: TH emission coils as a function of the analyzer angle. The black data points depict the measurements, and the blue solid line is a fitting function. In the first regime (greenish), the polarization of the nonlinear response is solely oriented along the *x* axis (same as the exciting electric field). In the second regime (light blue), the TH emission coils start to open (at about 1580 nm) and to rotate clockwise. This is a result of two contributions in the TH signal with perpendicular polarization and a phase between them. The largest opening of the coils is obtained at around 1660 nm. In the third regime (gray), the TH coil closes again and rotates slightly back. The largest rotation is recorded at around 1690 nm with a rotation larger than 45° indicating a stronger TH signal along the *y* axis. Note that some of the TH emission coils are scaled by a factor of 2 or 3 to account for the significant differences in the TH intensities.

no TH contribution polarized along the quadrupole wires is expected. Furthermore, a change in the polarization direction of the radiated TH for different displacements of the dipole rod and thus the coupling strength is also not expected.

A selection of the recorded polarization states is depicted as polar plots in Figure 3 (black data points), showing the orientation of the TH emission in the *xy* plane as a function of the polarizer angle and are scaled to their relative TH intensity. Note that some of the emission coils are scaled in order to account for the significant intensity differences.

Most generally, we have to assume two TH contributions of the sample, which are projected onto the analyzing polarizer: one polarized along the *x* and the other one along the *y* axis. As the incident radiation is coherent, also the radiated TH signals will be coherent resulting in an interference of the two contributions when taking the polarization-analyzing measure-

DOI: 10.1021/acsphotonics.9b00938
ACS Photonics XXXX, XXX, XXX−XXX

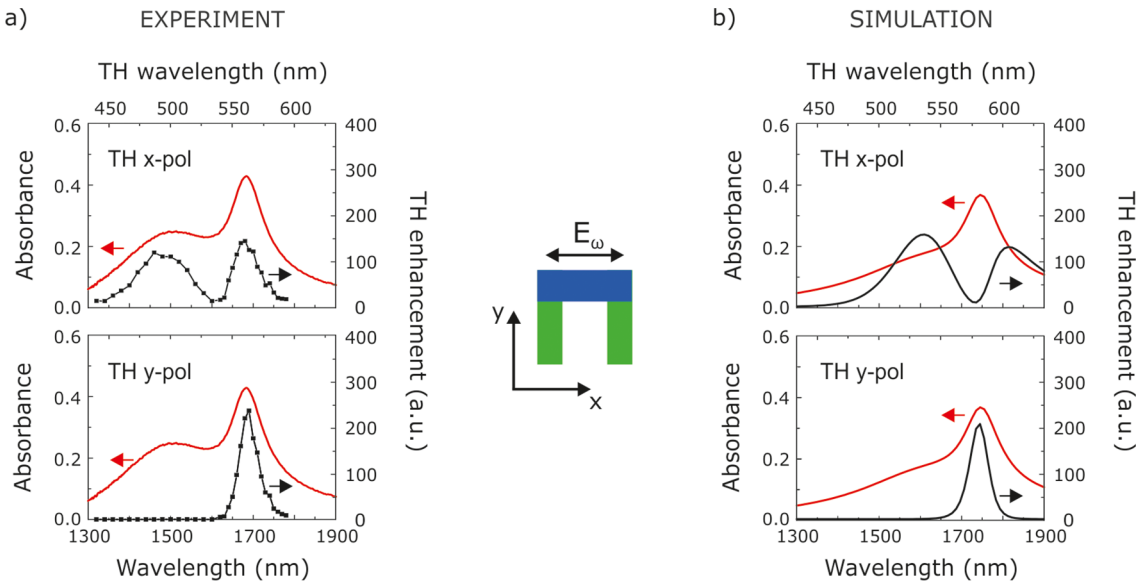

Figure 4. Top panels depict a comparison of the *x*-polarized TH emission obtained in the experiment (a) and by finite element simulation (b) assuming the design parameters. The red shift of the simulated TH response can be explained by the illumination geometry in the experiment (see Figure S5 in the Supporting Information). The lower panel compares the TH contribution in *y* polarization. Here, an additional asymmetry of 20 nm in the length of both quadrupole rods has been added to the simulation. The measurement and the simulation show a high qualitative agreement.

ment. The recorded TH signal in dependence of the analyzer angle (θ) will therefore be described by

$$I_{\mathrm{THG}}(\theta) \propto |A(\theta) + B(\theta)|^2$$

The strength of the contributions polarized in the *x* direction will be proportional to $\cos(\theta)$ and in the *y* direction to $\sin(\theta)$. When assuming a phase ϕ between the TH contributions, we obtain

$$I_{\mathrm{THG}}(\theta) \propto A^2[\cos(\theta)]^2 + B^2[\sin(\theta)]^2 + 2AB\cos(\theta)\sin(\theta)\cos(\phi)$$

A and *B* are the amplitudes of the electric field radiated along the *x* and *y* axes, respectively. The *x*- and *y* polarization components of the TH radiation exhibit a cosine and sine dependence on the polarizer angle θ, respectively. The function can be fitted to the experimental data, plotted as a solid blue line. From the fit, the respective amplitudes and the phase between the contributions can be extracted.

The top panel of Figure 3 illustrates again the TH enhancement curve as a function of wavelength as well as the absorbance of the nanoarray. Furthermore, three different regions are marked. In region I (light green), we find that the TH emission is polarized along the *x* axis and the intensity is increasing from 1340 to 1460 nm and then decreasing again for longer wavelength. In regime II (light blue), the emission coil starts to open at around 1600 nm and rotates clockwise. This rotation is the result of a contribution in the TH response with polarization along the *y* axis, while the opening can be explained by a phase ϕ between the two TH contributions. In general, the rotation visualizes the ratio of the fitting parameters A/B and thus the relative strength of both contributions. The maximum in the opening is observed at around 1660 nm showing a value of ϕ close to 90°. In region III (gray), the emission coil starts to close again, but yet further rotation toward the *y* axis is observed, which reaches a maximum at 1690 nm and then starts to rotate back toward the *x* axis. Further closing of the emission coil is observed when further increasing the excitation wavelength. The strongest rotation with a value of over 45° is recorded at 1690 nm, indicating an even stronger nonlinear response in the perpendicular polarization (with respect to the excitation wavelength). Moreover, the corresponding phase ϕ is plotted as a green dotted line in the upper panel of Figure 3, indicating a monotonically increasing phase ranging from 0° to almost 180° over the fundamental tuning range, while the first nonvanishing value of ϕ is observed at 1580 nm.

In general, and without any prior knowledge about the exact geometry of the structure, one cannot make any predictions about the polarization of the radiated TH signal and the relative strength. Using symmetry arguments, one can formulate general statements which contributions to an overall signal are allowed. Which contributions are nonzero, however, cannot be predicted using solely mathematical symmetry considerations. In our case, we have experimentally found that there are two contributions present, polarized along the *x* and *y* axis, respectively. From the detailed measurements depicted in Figure 3, we can decompose the overall signal and plot the contributions individually. The results are plotted in Figure 4a. We see that the contribution polarized along the *x* axis exhibits two peaks of enhanced TH generation, closely matching the shape of the absorbance spectrum. The contribution polarized along the *y* axis exhibits only one yet very prominent peak coinciding with the long wavelength mode. From this, we can in fact deduce the origin of the nonlinear contributions: The TH is radiated from local linear dipoles that drive the nonlinear ones, as has been shown in several publications.[53] Thus, the presence of a nonlinear emission points to the existence of two local linear dipole moments, one pointing in the *x* and one in the *y* direction. The *x* direction is dominated by the emission from the dipolar rod. Both hybrid modes of the coupled EIA structure have net dipole moments along this direction, and thus both modes are radiating. In a symmetric situation, one would not expect a net dipole moment in the *y*

DOI: 10.1021/acsphotonics.9b00938
ACS Photonics XXXX, XXX, XXX−XXX

direction as the two linear dipoles, which are associated with the two quadrupole wires, cancel each other out as they oscillate out of phase in the coupled system. The observation of a contribution polarized along these quadrupole wires is now a definitive indication of a structural asymmetry in this direction, that is, a length difference in the quadrupole wires or an unequal excitation strength in the coupling to the dipolar mode. This enables the coupled collective mode to exhibit a net dipole moment in the y direction and thus explains the radiated TH signal. It should be mentioned that this contribution is not caused by the in-phase oscillation of the two quadrupole rods, as this mode is energetically detuned to around 1480 nm as can be seen in Figure S3 of the Supporting Information. In addition, we can also rule out the influence of higher-order modes in the wavelength region of the TH, as there are no prominent modes present (Figure S4 of the Supporting Information). Moreover, we do not expect to observe any influence of the orientation of the individual gold grains, which have a size of roughly 25 nm, leading to an effectively pseudoamorphous state.

To support our conclusion of the influence of additional structural asymmetry, we performed finite-element simulations using the commercially available program COMSOL to investigate the influence of different types of structural asymmetry.

First, we performed COMSOL simulations using the design parameters from the experiment, given in Figure 4b. As expected, such a perfectly symmetric structure only leads to an emission along the long axis of the dipole (x axis), as seen in the upper panel. However, when introducing asymmetry to the structure (in addition to the already introduced asymmetry by shifting the dipole to quadrupole rod end), TH emission in the y direction is obtained. Here, we have assumed an asymmetry in the quadrupole rod lengths of 20 nm. The upper panel of Figure 4b depicts the absorbance and the simulated TH emission polarized along the dipole long axis. The simulated absorbance matches the spectral shape of the measured absorbance. Only a slight red shift of the spectra is observed as well as a lower modulation depth of the high-frequency mode. When comparing the experimental TH enhancement curves with the simulation, very good agreement can be noticed. The relative intensities are matching, and only a slight red shift of the simulation results with respect to the experimentally obtained data is observed. This red shift can be explained by the angled illumination geometry of the FTIR microscope, which is used for measuring the linear spectra. This illumination is different from a normal incidence plane wave excitation, which is the case for laser illumination in the nonlinear setup. We thus in fact expect a spectral shift between the two spectra (Figure S5 in the Supporting Information illustrates that a linear plasmon resonance measured with the FTIR setup is red-shifted with respect to the same resonance measured with the OPO as the white light source). When comparing the y polarization, we also find a very good agreement between experiment and simulation in relative height and spectral width. It should be mentioned that both TH enhancement axes in the simulation do have the same scale. Hence, by assuming the above-mentioned structural parameters, the relative TH intensities obtained for the different polarizations can be accurately predicted. As a matter of fact, even such small asymmetries, as assumed in the simulation, can tremendously influence the nonlinear response of the plasmonic system.

In the following, a more detailed picture of our simulation results is described. Figure 5 demonstrates the influence of

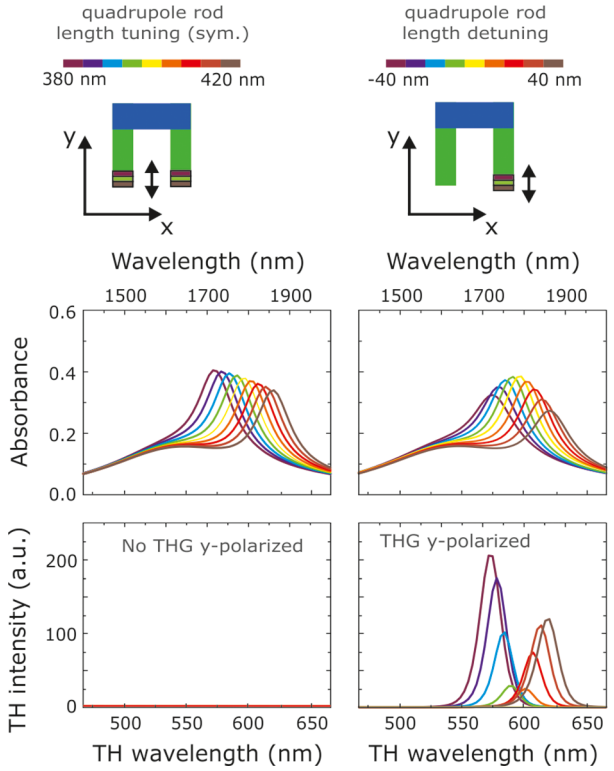

Figure 5. Simulated symmetric (left) and asymmetric (right) quadrupole rod length sweeps. In both cases, the linear absorbance spectra exhibit an increased splitting for increasing quadrupole rod length. From the linear response alone, it is hard to distinguish if only one quadrupole rod or both are increased in length. The lower panel depicts the corresponding TH emissions in the y direction. Here, only the asymmetric quadrupole length tuning shows a response due to the additional asymmetry in the system. This way, the nonlinear response reveals more information than the linear spectra can.

quadrupole rod length tuning on the linear and nonlinear optical spectra of the EIA structure. Both, symmetric and asymmetric rod length tuning are performed. As can be seen in the upper panels, the linear absorbance spectra exhibit very similar spectral shifts of the two different modes when increasing the quadrupole rod length from 380 to 420 nm in the symmetric as well as the asymmetric rod length tuning (detuning of rod length from −40 to 40 nm). Both modes shift red and the spectral splitting is increasing. Consequently, by solely observing the linear absorbance spectra, one cannot easily differentiate between the symmetric and the asymmetric structure, and the same holds true when investigating solely the x polarization of the nonlinear response at the TH wavelength (cf. Figure S6 in the Supporting Information). However, while the symmetric quadrupole length tuning leads to zero TH emission along the y axis, as the quadrupole is perfectly symmetric and thus completely dark, the asymmetric tuning leads to such a radiation of the TH into the far-field. This is illustrated in a direct comparison in the lower panel of Figure 5. Interestingly, the strongest TH signal in y polarization is not obtained for the strongest asymmetry. We suspect that this is caused by the decreasing quality factor $Q = \frac{\lambda}{\Delta\lambda}$ of the quadrupole resonance and the reduced spectral overlap of

DOI: 10.1021/acsphotonics.9b00938
ACS Photonics XXXX, XXX, XXX−XXX

both modes. Thus, the *y*-polarized TH intensity radiated in the *y* direction is a compromise between adding additional asymmetry to the system and therefore allowing for radiation into the far-field and keeping the quality factor of the resonance high.

As another example of the influence of the additional asymmetry, Figure 6 illustrates the simulation results on the influence of the shift in the *x* direction of the dipole out of the center position toward one of the quadrupole rods. In the linear absorbance spectra, hardly any change is visible when increasing the shift from 0 to 50 nm. The same holds true for the *x* polarization of the TH emission (center panel of Figure 6). Again as depicted in the lower panel of Figure 6, a TH signal in *y* polarization is emerging as soon as displacing the dipole rod in the *x* direction, as the coupling to the two quadrupole rods becomes asymmetric, which leads to a partially bright quadrupolar mode. Within our simulation parameters, an increase in this TH contribution is observed for further increasing displacement of the dipole rod. However, here the TH intensity in the *y* direction is not as strong as it is in the asymmetric tuning of the quadrupole rod length. It should be mentioned that the orientation of the angular emission of the TH signal changes when shifting the dipole rod in the *x* direction due to the increasing *y*-polarized TH radiation and the relative phase ϕ between both contributions.

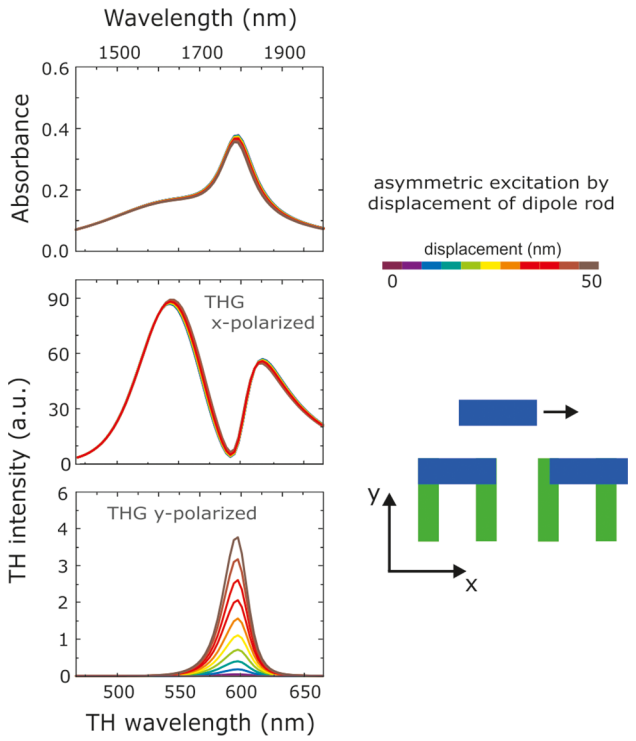

Figure 6. Simulated asymmetric dipole position sweep. The linear absorbance spectra indicate almost no change when shifting the dipole out of the center toward one of the quadrupole rods. The same is observed in the TH response in the *x* direction. Again, the TH signal polarized along the *y* axis of the system reveals an increased intensity with increasing shift of the dipole out of its center position. Obviously, the nonlinear response reveals more information about the structure than the linear spectra and thus can be used to detect asymmetries in structure.

The simulations results shown in Figures 5 and 6 underpin that the radiated TH polarized along the *y* axis stems from a length difference of the two quadrupole wires. Inspection of SEM images indeed suggests a consistent length difference between the two wires. We note that due to the polymer overcoat and the accompanied lower resolution, a quantitative evaluation of the SEM images is not possible. In order for the effect to persist, this "defect" needs to be identical for every individual dolmen structure. Indeed, we find that the left wire is always approximately 20 nm shorter than the right one. We ascribe this effect to the sequential exposure of the elements, which occurs in the same order, causing this effect. Accidental or deliberate misalignment of the two layers would rather result in a warping of the two layers with respect to one another. This warping will manifest itself in a Moire-like pattern, which would make the resulting nonlinear response even more complex, as can be seen in similar systems studying fluorescence.[60] Further possible asymmetries are, as already noted above, a rotation of the dipole around its center position in the *xy* plane. It should be mentioned that every fabricated nanostructure will of course exhibit a superposition of the introduced asymmetries as a consequence of the imperfections in the fabrication process as well as in the measurement setup. In principle, even more sophisticated methods can be used to perform the simulations in which the propagation of the TH signal from the near- to the far-field is taken into account.[61,62]

Our findings indicate that the nonlinear response can resolve geometrical asymmetries or structural imperfections, which hardly manifest themselves in the linear regime, but which are unambiguously present in the nonlinear regime. Recently, it has also been shown that symmetry breaking can enhance the third-order nonlinearity in nanotips using high field gradients.[63,64]

In conclusion, we have performed TH spectroscopy on the plasmonic analog of EIA. This structure offers several distinct tuning parameters, which can be used to manipulate the linear as well as the nonlinear optical response of the system. Our findings indicate that the linear properties can hardly resolve structural asymmetry which, however, manifests itself unambiguously in the *nonlinear* response of the system. Additionally, our study provides further insight into the influence of coupling strength and phase relations in the nonlinear optical response of complex plasmonic structures. We envision that our findings will stimulate further research into phase tuning, structural symmetries, and manipulation in nonlinear plasmonic systems in order to fully exploit the ability to tailor the linear and specifically the nonlinear optical properties of nanostructured matter.

■ ASSOCIATED CONTENT

Supporting Information

The Supporting Information is available free of charge on the ACS Publications website at DOI: 10.1021/acsphotonics.9b00938.

Figure S1, signal spectra of the OPO; Figure S2, coupled harmonic oscillator model in comparison to experimentally obtained TH spectra; Figure S3, linear plasmon resonances of the quadrupole rods (symmetric mode); Figure S4, linear plasmon resonances in the TH wavelength range of the EIA structure; Figure S5, dependence of the plasmon resonance on different light sources; and Figure S6, comparison of absorbance and TH efficiencies of symmetric and asymmetric quadrupole rod length tuning (PDF)

DOI: 10.1021/acsphotonics.9b00938
ACS Photonics XXXX, XXX, XXX−XXX

AUTHOR INFORMATION

Corresponding Author

*E-mail: j.krauth@pi4.uni-stuttgart.de.

ORCID

Joachim Krauth: 0000-0001-9683-762X
Markus Lippitz: 0000-0003-1218-6511
Thomas Weiss: 0000-0002-4991-6779
Mario Hentschel: 0000-0002-6882-4183

Notes

The authors declare no competing financial interest.

ACKNOWLEDGMENTS

We thank Julian Karst for helpful discussions and Tobias Steinle for technical support. The authors gratefully acknowledge financial support by the ERC Advanced Grant (COMPLEXPLAS), Deutsche Forschungsgemeinschaft (Grant SPP1839), and Baden-Württemberg Stiftung, MWK Baden-Württemberg (IQST, ZAQuant, Juniorprofessurenprogramm).

REFERENCES

(1) Kauranen, M.; Zayats, A. V. Nonlinear Plasmonics. *Nat. Photonics* **2012**, *6* (11), 737−748.

(2) O'Brien, K.; Suchowski, H.; Rho, J.; Salandrino, A.; Kante, B.; Yin, X.; Zhang, X. Predicting Nonlinear Properties of Metamaterials from the Linear Response. *Nat. Mater.* **2015**, *14* (4), 379−383.

(3) Butet, J.; Brevet, P.-F.; Martin, O. J. F. Optical Second Harmonic Generation in Plasmonic Nanostructures: From Fundamental Principles to Advanced Applications. *ACS Nano* **2015**, *9* (11), 10545−10562.

(4) Obermeier, J.; Schumacher, T.; Lippitz, M. Nonlinear Spectroscopy of Plasmonic Nanoparticles. *Adv. Phys. X* **2018**, *3* (1), 1454341.

(5) Metzger, B.; Hentschel, M.; Lippitz, M.; Giessen, H. Third-Harmonic Spectroscopy and Modeling of the Nonlinear Response of Plasmonic Nanoantennas. *Opt. Lett.* **2012**, *37* (22), 4741−4743.

(6) Gentile, M.; Hentschel, M.; Taubert, R.; Guo, H.; Giessen, H.; Fiebig, M. Investigation of the Nonlinear Optical Properties of Metamaterials by Second Harmonic Generation. *Appl. Phys. B: Lasers Opt.* **2011**, *105* (1), 149−162.

(7) Klein, M. W.; Enkrich, C.; Wegener, M.; Linden, S. Second-Harmonic Generation from Magnetic Metamaterials. *Science* **2006**, *313* (5786), 502−504.

(8) Shi, L.; Iwan, B.; Nicolas, R.; Ripault, Q.; Andrade, J. R. C.; Han, S.; Kim, H.; Boutu, W.; Franz, D.; Heidenblut, T.; Reinhardt, C.; Bastiaens, B.; Nagy, T.; Babushkin, I.; Morgner, U.; Kim, S.-W.; Steinmeyer, G.; Merdji, H.; Kovacev, M. Self-Optimization of Plasmonic Nanoantennas in Strong Femtosecond Fields. *Optica* **2017**, *4* (9), 1038.

(9) Fischer, H.; Martin, O. J. F. Engineering the Optical Response of Plasmonic Nanoantennas. *Opt. Express* **2008**, *16* (12), 9144−9154.

(10) Hentschel, M.; Utikal, T.; Giessen, H.; Lippitz, M. Quantitative Modeling of the Third Harmonic Emission Spectrum of Plasmonic Nanoantennas. *Nano Lett.* **2012**, *12* (7), 3778−3782.

(11) Hentschel, M.; Schäferling, M.; Weiss, T.; Liu, N.; Giessen, H. Three-Dimensional Chiral Plasmonic Oligomers. *Nano Lett.* **2012**, *12* (5), 2542−2547.

(12) Rahmani, M.; Shorokhov, A. S.; Hopkins, B.; Miroshnichenko, A. E.; Shcherbakov, M. R.; Camacho-Morales, R.; Fedyanin, A. A.; Neshev, D. N.; Kivshar, Y. S. Nonlinear Symmetry Breaking in Symmetric Oligomers. *ACS Photonics* **2017**, *4*, 454−461.

(13) Huttunen, M. J.; Bautista, G.; Decker, M.; Linden, S.; Wegener, M.; Kauranen, M. Nonlinear Chiral Imaging of Subwavelength-Sized Twisted-Cross Gold Nanodimers [Invited]. *Opt. Mater. Express* **2011**, *1* (1), 46−56.

(14) Wurtz, G. A.; Pollard, R.; Hendren, W.; Wiederrecht, G. P.; Gosztola, D. J.; Podolskiy, V. A.; Zayats, A. V. Designed Ultrafast Optical Nonlinearity in a Plasmonic Nanorod Metamaterial Enhanced by Nonlocality. *Nat. Nanotechnol.* **2011**, *6* (2), 107−111.

(15) Liu, N.; Giessen, H. Coupling Effects in Optical Metamaterials. *Angew. Chem., Int. Ed.* **2010**, *49* (51), 9838−9852.

(16) Ye, W.; Zeuner, F.; Li, X.; Reineke, B.; He, S.; Qiu, C.-W.; Liu, J.; Wang, Y.; Zhang, S.; Zentgraf, T. Spin and Wavelength Multiplexed Nonlinear Metasurface Holography. *Nat. Commun.* **2016**, *7*, 11930.

(17) Liu, S.; Vabishchevich, P. P.; Vaskin, A.; Reno, J. L.; Keeler, G. A.; Sinclair, M. B.; Staude, I.; Brener, I. An All-Dielectric Metasurface as a Broadband Optical Frequency Mixer. *Nat. Commun.* **2017**, *9* (1), 1−6.

(18) Niesler, F. B. P.; Feth, N.; Linden, S.; Wegener, M. Second-Harmonic Optical Spectroscopy on Split-Ring-Resonator Arrays. *Opt. Lett.* **2011**, *36* (9), 1533−1535.

(19) Linden, S.; Niesler, F. B. P.; Förstner, J.; Grynko, Y.; Meier, T.; Wegener, M. Collective Effects in Second-Harmonic Generation from Split-Ring-Resonator Arrays. *Phys. Rev. Lett.* **2012**, *109* (1), 015502.

(20) Aouani, H.; Navarro-Cia, M.; Rahmani, M.; Sidiropoulos, T. P. H. H.; Hong, M.; Oulton, R. F.; Maier, S. A. Multiresonant Broadband Optical Antennas As Efficient Tunable Nanosources of Second Harmonic Light. *Nano Lett.* **2012**, *12* (9), 4997−5002.

(21) Lippitz, M.; van Dijk, M. A.; Orrit, M. Third-Harmonic Generation from Single Gold Nanoparticles. *Nano Lett.* **2005**, *5*, 799−802.

(22) Utikal, T.; Zentgraf, T.; Paul, T.; Rockstuhl, C.; Lederer, F.; Lippitz, M.; Giessen, H. Towards the Origin of the Nonlinear Response in Hybrid Plasmonic Systems. *Phys. Rev. Lett.* **2011**, *106*, 133901.

(23) Renger, J.; Quidant, R.; Van Hulst, N.; Novotny, L. Surface-Enhanced Nonlinear Four-Wave Mixing. *Phys. Rev. Lett.* **2010**, *104* (4), 046803.

(24) Palomba, S.; Danckwerts, M.; Novotny, L. Nonlinear Plasmonics with Gold Nanoparticle Antennas. *J. Opt. A: Pure Appl. Opt.* **2009**, *11* (11), 114030.

(25) Danckwerts, M.; Novotny, L. Optical Frequency Mixing at Coupled Gold Nanoparticles. *Phys. Rev. Lett.* **2007**, *98* (2), 026104.

(26) Zhang, Y.; Wen, F.; Zhen, Y.-R.; Nordlander, P.; Halas, N. J. Coherent Fano Resonances in a Plasmonic Nanocluster Enhance Optical Four-Wave Mixing. *Proc. Natl. Acad. Sci. U. S. A.* **2013**, *110* (23), 9215−9219.

(27) Hanke, T.; Krauss, G.; Träutlein, D.; Wild, B.; Bratschitsch, R.; Leitenstorfer, A. Efficient Nonlinear Light Emission of Single Gold Optical Antennas Driven by Few-Cycle near-Infrared Pulses. *Phys. Rev. Lett.* **2009**, *103* (25), 257404.

(28) Zhang, Y.; Grady, N. K.; Ayala-Orozco, C.; Halas, N. J. Three-Dimensional Nanostructures as Highly Efficient Generators of Second Harmonic Light. *Nano Lett.* **2011**, *11* (12), 5519−5523.

(29) Harutyunyan, H.; Volpe, G.; Quidant, R.; Novotny, L. Enhancing the Nonlinear Optical Response Using Multifrequency Gold-Nanowire Antennas. *Phys. Rev. Lett.* **2012**, *108* (21), 217403.

(30) Hegenbarth, R.; Steinmann, A.; Sarkisov, S.; Giessen, H. Milliwatt-Level Mid-Infrared (10.5−16.5 Mm) Difference Frequency Generation with a Femtosecond Dual-Signal-Wavelength Optical Parametric Oscillator. *Opt. Lett.* **2012**, *37* (17), 3513−3515.

(31) Neacsu, C. C.; Reider, G. A.; Raschke, M. B. Second-Harmonic Generation from Nanoscopic Metal Tips: Symmetry Selection Rules for Single Asymmetric Nanostructures. *Phys. Rev. B: Condens. Matter Mater. Phys.* **2005**, *71*, 201402.

(32) Ko, K. D.; Kumar, A.; Fung, K. H.; Ambekar, R.; Liu, G. L.; Fang, N. X.; Toussaint, K. C. Nonlinear Optical Response from Arrays of Au Bowtie Nanoantennas. *Nano Lett.* **2011**, *11* (1), 61−65.

(33) Metzger, B.; Hentschel, M.; Giessen, H. Probing the Near-Field of Second-Harmonic Light around Plasmonic Nanoantennas. *Nano Lett.* **2017**, *17* (3), 1931−1937.

(34) Linnenbank, H.; Grynko, Y.; Förstner, J.; Linden, S. Second Harmonic Generation Spectroscopy on Hybrid Plasmonic/Dielectric Nanoantennas. *Light: Sci. Appl.* **2016**, *5* (1), e16013.

(35) Czaplicki, R.; Zdanowicz, M.; Koskinen, K.; Laukkanen, J.; Kuittinen, M.; Kauranen, M. Dipole Limit in Second-Harmonic

DOI: 10.1021/acsphotonics.9b00938
ACS Photonics XXXX, XXX, XXX−XXX

Generation from Arrays of Gold Nanoparticles. *Opt. Express* **2011**, *19* (27), 26866−26871.
(36) Muskens, O. L.; Del Fatti, N.; Vallée, F. Femtosecond Response of a Single Metal Nanoparticle. *Nano Lett.* **2006**, *6* (3), 552−556.
(37) Fedutik, Y.; Temnov, V. V.; Schöps, O.; Woggon, U.; Artemyev, M. V. Exciton-Plasmon-Photon Conversion in Plasmonic Nanostructures. *Phys. Rev. Lett.* **2007**, *99* (13), 136802.
(38) Aouani, H.; Rahmani, M.; Navarro-Cía, M.; Maier, S. A. Third-Harmonic-Upconversion Enhancement from a Single Semiconductor Nanoparticle Coupled to a Plasmonic Antenna. *Nat. Nanotechnol.* **2014**, *9* (4), 290−294.
(39) von Cube, F.; Irsen, S.; Diehl, R.; Niegemann, J.; Busch, K.; Linden, S. From Isolated Metaatoms to Photonic Metamaterials: Evolution of the Plasmonic Near-Field. *Nano Lett.* **2013**, *13* (2), 703−708.
(40) Prodan, E.; Radloff, C.; Halas, N. J.; Nordlander, P. A Hybridization Model for the Plasmon Response of Complex Nanostructures. *Science (Washington, DC, U. S.)* **2003**, *302* (5644), 419−422.
(41) Nordlander, P.; Oubre, C.; Prodan, E.; Li, K.; Stockman, M. I. Plasmon Hybridization in Nanoparticle Dimers. *Nano Lett.* **2004**, *4* (5), 899−903.
(42) Thyagarajan, K.; Butet, J.; Martin, O. J. F. Ultrasensitive Optical Shape Characterization of Gold Nanoantennas Using Second Harmonic Generation. *Nano Lett.* **2013**, *13*, 1847.
(43) Muskens, O. L.; Giannini, V.; Sánchez-Gil, J. A.; Gómez Rivas, J. Strong Enhancement of the Radiative Decay Rate of Emitters by Single Plasmonic Nanoantennas. *Nano Lett.* **2007**, *7* (9), 2871−2875.
(44) Metzger, B.; Schumacher, T.; Hentschel, M.; Lippitz, M.; Giessen, H. Third Harmonic Mechanism in Complex Plasmonic Fano Structures. *ACS Photonics* **2014**, *1* (6), 471−476.
(45) Liu, N.; Langguth, L.; Weiss, T.; Kästel, J.; Fleischhauer, M.; Pfau, T.; Giessen, H. Plasmonic Analogue of Electromagnetically Induced Transparency at the Drude Damping Limit. *Nat. Mater.* **2009**, *8* (9), 758−762.
(46) Rahmani, M.; Tahmasebi, T.; Lin, Y.; Lukiyanchuk, B.; Liew, T. Y. F.; Hong, M. H. Influence of Plasmon Destructive Interferences on Optical Properties of Gold Planar Quadrumers. *Nanotechnology* **2011**, *22* (24), 245204.
(47) Fan, J. A.; Bao, K.; Wu, C.; Bao, J.; Bardhan, R.; Halas, N. J.; Manoharan, V. N.; Shvets, G.; Nordlander, P.; Capasso, F. Fano-like Interference in Self-Assembled Plasmonic Quadrumer Clusters. *Nano Lett.* **2010**, *10* (11), 4680−4685.
(48) Muller, E. A.; Pollard, B.; Bechtel, H. A.; Adato, R.; Etezadi, D.; Altug, H.; Raschke, M. B. Nanoimaging and Control of Molecular Vibrations through Electromagnetically Induced Scattering Reaching the Strong Coupling Regime. *ACS Photonics* **2018**, *5* (9), 3594−3600.
(49) Taubert, R.; Hentschel, M.; Kästel, J.; Giessen, H. Classical Analog of Electromagnetically Induced Absorption in Plasmonics. *Nano Lett.* **2012**, *12*, 1367−1371.
(50) Zhang, S.; Ye, Z.; Wang, Y.; Park, Y.; Bartal, G.; Mrejen, M.; Yin, X.; Zhang, X. Anti-Hermitian Plasmon Coupling of an Array of Gold Thin-Film Antennas for Controlling Light at the Nanoscale. *Phys. Rev. Lett.* **2012**, *109* (19), 193902.
(51) Ren, X.; Jha, P. K.; Wang, Y.; Zhang, X. Nonconventional Metasurfaces: From Non-Hermitian Coupling, Quantum Interactions, to Skin Cloak. *Nanophotonics* **2018**, *7* (6), 1233−1243.
(52) Taubert, R.; Hentschel, M.; Giessen, H. Plasmonic Analog of Electromagnetically Induced Absorption: Simulations, Experiments, and Coupled Oscillator Analysis. *J. Opt. Soc. Am. B* **2013**, *30* (12), 3123−3134.
(53) Wolf, D.; Schumacher, T.; Lippitz, M. Shaping the Nonlinear near Field. *Nat. Commun.* **2016**, *7*, 10361.
(54) Albrecht, G.; Hentschel, M.; Kaiser, S.; Giessen, H. Refractory Plasmonics without Refractory Materials. *Nano Lett.* **2017**, *17*, 6402−6408.
(55) Olmon, R. L.; Slovick, B.; Johnson, T. W.; Shelton, D.; Oh, S.-H.; Boreman, G. D.; Raschke, M. B. Optical Dielectric Function of Gold. *Phys. Rev. B: Condens. Matter Mater. Phys.* **2012**, *86* (23), 235147.
(56) Metzger, B.; Steinmann, A.; Hoos, F.; Pricking, S.; Giessen, H. Compact Laser Source for High-Power White-Light and Widely Tunable Sub 65 Fs Laser Pulses. *Opt. Lett.* **2010**, *35* (23), 3961.
(57) Sudmeyer, T.; Aus der Au, J.; Paschotta, R.; Keller, U.; Smith, P. G. R.; Ross, G. W.; Hanna, D. C. Femtosecond Fiber-Feedback Optical Parametric Oscillator. *Opt. Lett.* **2001**, *26* (5), 304−306.
(58) Mörz, F.; Steinle, T.; Steinmann, A.; Giessen, H. Multi-Watt Femtosecond Optical Parametric Master Oscillator Power Amplifier at 43 MHz. *Opt. Express* **2015**, *23* (18), 23960−23967.
(59) Krauth, J.; Giessen, H.; Hentschel, M. Wavelength-Dependent Third-Harmonic Generation in Plasmonic Gold Nanoantennas: Quantitative Determination of the d-Band Influence. *ACS Photonics* **2018**, *5* (5), 1863−1870.
(60) Koller, D. M.; Hohenester, U.; Hohenau, A.; Ditlbacher, H.; Reil, F.; Galler, N.; Aussenegg, F. R.; Leitner, A.; Trügler, A.; Krenn, J. R. Superresolution Moiré Mapping of Particle Plasmon Modes. *Phys. Rev. Lett.* **2010**, *104* (14), 143901.
(61) Nesterov, M. L.; Schäferling, M.; Weber, K.; Neubrech, F.; Giessen, H.; Weiss, T. Line-Current Model for Deriving the Wavelength Scaling of Linear and Nonlinear Optical Properties of Thin Elongated Metallic Rod Antennas. *J. Opt. Soc. Am. B* **2018**, *35* (7), 1482.
(62) Defrance, J.; Schäferling, M.; Weiss, T. Modeling of Second-Harmonic Generation in Periodic Nanostructures by the Fourier Modal Method with Matched Coordinates. *Opt. Express* **2018**, *26* (11), 13746.
(63) Kravtsov, V.; AlMutairi, S.; Ulbricht, R.; Kutayiah, A. R.; Belyanin, A.; Raschke, M. B. Enhanced Third-Order Optical Nonlinearity Driven by Surface-Plasmon Field Gradients. *Phys. Rev. Lett.* **2018**, *120* (20), 203903.
(64) Kravtsov, V.; Ulbricht, R.; Atkin, J. M.; Raschke, M. B. Plasmonic Nanofocused Four-Wave Mixing for Femtosecond near-Field Imaging. *Nat. Nanotechnol.* **2016**, *11* (5), 459−464.

DOI: 10.1021/acsphotonics.9b00938
ACS Photonics XXXX, XXX, XXX−XXX